Article

EARTHQUAKE SPECTRA

Earthquake Spectra
1–27

DOI: 10.1177/8755293019878185
journals.sagepub.com/home/eqs
SAGE

Ergodic site amplification model for central and eastern North America

Jonathan P Stewart, M.EERI[1], Grace A Parker, M.EERI[1], Gail M Atkinson, M.EERI[2], David M Boore[3], Youssef MA Hashash, M.EERI[4], and Walter J Silva, M.EERI[5]

Abstract

The United States Geological Survey national seismic hazard maps have historically been produced for a reference site condition of V_{S30} = 760 m/s. For other site conditions, site factors are used, which heretofore have been developed using ground motion data and simulations for shallow earthquakes in active tectonic regions. Research results from the Next Generation Attenuation–East (NGA-East) project, as well as previous and contemporaneous related research, demonstrate different levels of site amplification in central and eastern North America (CENA) as compared to active regions. We provide recommendations for modeling of ergodic site amplification in CENA based primarily on research results from the literature. The recommended model has three additive terms in natural logarithmic units. Two describe linear site amplification: an empirically constrained V_{S30}-scaling term relative to a 760 m/s reference and a simulation-based term to adjust site amplification from the 760 m/s reference to the CENA reference of V_S = 3000 m/s. The third term is a nonlinear model that is described in a companion document. All median model components are accompanied by epistemic uncertainty models.

Keywords

Ground motion model, Site amplification, seismic hazard maps

Date received: 26 January 2019; accepted: 13 June 2019

[1]University of California, Los Angeles, Los Angeles, CA
[2]Western University, London, ON, Canada (retired)
[3]Seismologist, Los Altos, CA
[4]University of Illinois–Urbana Champaign, Urbana, IL
[5]Pacific Engineering and Analysis, El Cerrito, CA

Corresponding author:
Jonathan P Stewart, University of California, Los Angeles, Los Angeles, CA 90095.
Email: jstewart@seas.ucla.edu

Introduction

The Next Generation Attenuation–East (NGA-East) project produced ground motion models (GMMs) for central and eastern North America (CENA) (Goulet et al., 2017, 2018; Pacific Earthquake Engineering Research Center (PEER), 2015a, 2015b). The majority of these models provide ground motion intensity measure predictions as a function of earthquake source and wave propagation path for sites with a hard rock reference condition defined as shear-wave velocity V_s = 3000 m/s and site decay parameter κ_0 = 0.006 s (Hashash et al., 2014). Some of those models also provide ground motions for the National Earthquake Hazards Reduction Program (NEHRP) B/C boundary condition of V_{S30} = 760 m/s, where V_{S30} is the time-averaged shear-wave velocity in the uppermost 30 m of the site.

The United States Geological Survey (USGS) national seismic hazard maps present ground motion intensity measures with specified probabilities of exceedance over a 50-year time period (Petersen et al., 2015). A major recent update of these maps utilized NGA-East GMMs for the CENA region (Petersen et al., 2020). A special consideration for this update is that maps are being produced for a variety of site conditions (represented by a range of V_{S30}) and periods, as a result of recommendations from Project 17 (Building Seismic Safety Council (BSSC), 2018). This is a departure from past practice in which the maps were produced for the NEHRP B/C boundary site condition (V_{S30} = 760 m/s) and the ground motion intensity measures of peak acceleration and 5% damped pseudo-spectral acceleration (PSA) at oscillator periods of 0.2 and 1.0 s.

An expert panel (comprising the authors of this article, plus Robert Darragh) was convened in 2016 with a charge to review alternate site amplification models for CENA and to provide recommendations to the USGS regarding estimation of median site effects and their epistemic uncertainties. This work required that the recommended models be based on V_{S30} as the sole predictive variable for site response, for compatibility with the NEHRP site categories A–E used in current practice (which are defined for ranges of V_{S30}). The consideration of models conditioned on alternative or additional parameters such as depth or dominant site period was beyond our scope; the panel recognizes the uncertainty reduction that can be achieved using such parameters and encourages their use in site-specific studies and in future updates of the national maps. The panel developed initial recommendations that were presented in two reports in June 2017 (Hashash et al., 2017; Stewart et al., 2017b). As the USGS implemented these models, feedback was provided to the panel from USGS scientists and via public comment, which resulted in several adjustments. This article presents models ultimately recommended by the panel and implemented for the national maps by USGS, including adjustments since June 2017. We explain the reasoning behind the model formulation and the definition of epistemic uncertainties. The emphasis here is on the linear components of the model, which presented the principal technical challenges. The nonlinear component of the model and its uncertainty are given in a companion paper (Hashash et al., this issue), which updates a prior report (Hashash et al., 2017). We do not provide a model for aleatory variability, which was addressed by Goulet et al. (2017) for reference rock. Stewart et al. (2019) provided recommendations to USGS for the significant site-to-site variability that is present at soil sites in CENA, many of which have a high-frequency response peak.

Prior work

Empirical site amplification studies

Empirical site amplification models, while numerous and well-established in some active tectonic regions, have only recently been developed for stable continental regions like

CENA. This is due to a number of factors, including a lack of V_{S30} information at seismographic sites in CENA (addressed in NGA-East by the development of a regional, proxy-based V_{S30}-prediction model; Parker et al., 2017). Parker et al. (2019) present an empirical linear site amplification model, conditioned on V_{S30}, which was developed by the NGA-East Geotechnical Working Group (GWG). Hassani and Atkinson (2016b) derived the frequency of peaks in H/V spectral ratios using CENA data and used those peak frequencies as predictive parameters for analysis of site effects. They find that the data-derived peak frequencies are more effective than V_{S30} at predicting site effects in the CENA data. Additional literature review on CENA empirical site amplification is presented by Parker et al. (2019). The panel considered the GWG and Hassani and Atkinson (2016b) empirical models.

Simulation-based site amplification

As a result of limited empirical site amplification studies, previous work has largely investigated site amplification using simulations of one-dimensional (1D) shear-wave propagation through shallow sediments (also known as ground response analysis (GRA)). The panel considered four simulation-based studies (or collections of studies) for CENA. The first was by Hwang et al. (1997) and was targeted at the CENA region generally. They computed site coefficients for CENA, akin to those in the NEHRP Provisions, using equivalent-linear GRA with simulated input motions for five unspecified magnitude–distance combinations generated using the method described in Hwang and Huo (1994). They considered five representative profiles for NEHRP site Classes A–E (profiles shown in Lin et al., 1996). Their results for site Classes A and B (rock sites) match those in the 1992 NEHRP Provisions. Site factors for Classes C–E are generally higher. Figure 1a shows their recommended amplification for Classes C–E for a rock peak acceleration level of 0.3*g*, and Figure 1b shows the variation of Class D amplification with shaking amplitude.

The second study by Darragh et al. (2015) also computed site amplification using equivalent-linear GRA for NEHRP site Classes A–E. Amplification was computed relative to a 3.0 km/s reference condition. Input ground motion conditions are for magnitude (**M**) 6.5 earthquakes and a distance range of 6–290 km.

The third group of studies evaluated site effects for the Mississippi embayment region (Hashash et al., 2008; Hashash and Park, 2001; Park and Hashash, 2005a, 2005b; Romero and Rix, 2001). The literature for this region is substantial and has arguably been supplanted by more recent work by the NGA-East GWG as presented in Harmon et al. (2019a, 2019b). The GWG study considered a wide variety of site conditions and used fully nonlinear GRA. Input motions cover an approximate magnitude range of 4.5–7.5 and distance range of 0–250 km (Harmon et al., 2019b). Models were provided for linear effects, including V_{S30}-scaling and effects of site period and sediment depth. A model for nonlinear effects was also provided.

The fourth CENA study is from Aboye et al. (2015), who developed site factors for Charleston, South Carolina. They developed a series of reference V_S profiles assuming different Quaternary layer thicknesses and taking layer velocities from measurements in Quaternary and Tertiary lithologic units. After introducing V_S profile variability, they adopt 56 profiles, placed over a half-space with $V_S = 700$ m/s. They used simulated input motions for **M** 7.2–7.4 earthquakes at source distances of 6–36 km and applied both equivalent-linear and nonlinear GRA methods. Figure 2 shows representative results for amplification of 0.2 s PSA.

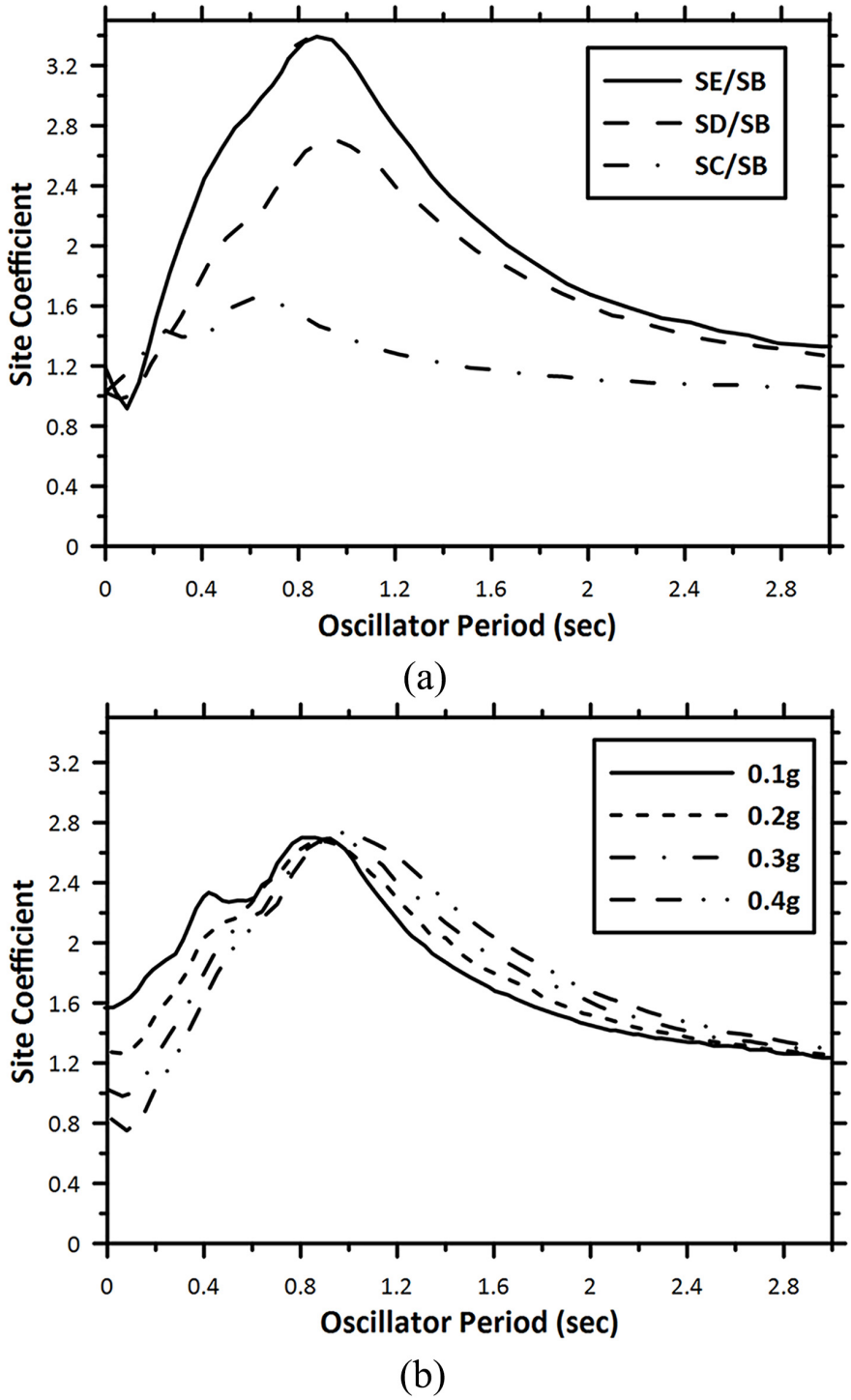

Figure 1. (a) CENA site amplification for Classes C, D, and E relative to Class B for rock PGA 0.3*g* and (b) dependence of Class D amplification on rock PGA.
Source: Adapted from Hwang et al. (1997).

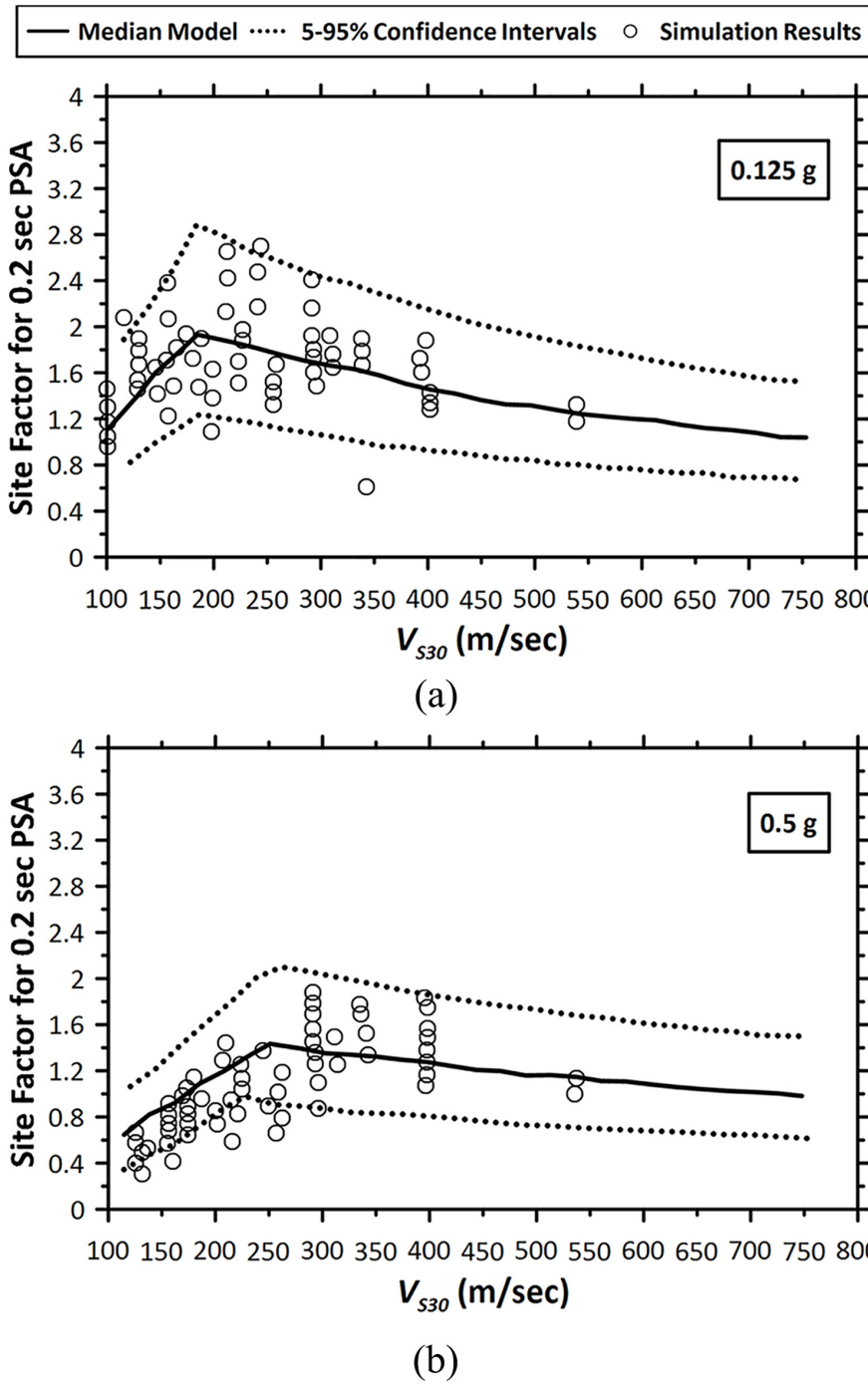

Figure 2. Computed amplification of 0.2 s PSA for Charleston, South Carolina by Aboye et al. (2015) for input ground motion intensity for rock of 0.2 s PSA: (a) 0.125*g* and (b) 0.5*g*.

Recommended model

This section provides a succinct summary of the recommended model. Justification for the model form and coefficients are provided in subsequent sections.

Approach

Site amplification relative to a V_S = 3000 m/s reference condition is denoted F_S and is provided in natural log units. The recommended model has three additive components representing (1) V_{S30}-scaling (relative to V_{S30} = 760 m/s), (2) amplification at the V_{S30} = 760 m/s site condition relative to 3000 m/s, and (3) nonlinear effects. The first two components are independent of shaking amplitude and hence are described as linear and are denoted F_{lin}. The nonlinear component is denoted F_{nl} and is also in natural log units. The total amplification is the sum:

$$F_S = F_{lin} + F_{nl} \tag{1}$$

where

$$F_{lin} = F_V(V_{S30}, T) + F_{760}(V_{S30}, T) \tag{2}$$

where F_V is the V_{S30}-scaling term and F_{760} represents amplification at the V_{S30} = 760 m/s site condition relative to a 3000 m/s reference condition. Recommended median models for F_V and F_{760} are given in the following sub-sections along with their epistemic uncertainties. Hashash et al. (this issue) present the model for nonlinear effects and related uncertainties. Equation 2 is suitable for use with a GMM having a reference condition of V_S = 3000 m/s. It can be used with a GMM having a reference condition of V_{S30} = 760 m/s by dropping the F_{760} term from Equation 2.

For the F_V term, the recommended model is largely controlled by empirical observations (NGA-East ground motion data). The F_{760} and F_{nl} terms are controlled by simulations. The rationale for this approach is discussed in the "Summary and discussion" section of this article.

V_{S30}-scaling model

The V_{S30}-scaling model is quad-linear in log–log space, as given below:

$$F_V = \begin{cases} c\ln\left(\frac{V_1}{V_{ref}}\right) & V_\ell < V_{S30} \leq V_1 \\ c\ln\left(\frac{V_{S30}}{V_{ref}}\right) & V_1 < V_{S30} \leq V_2 \\ c\ln\left(\frac{V_2}{V_{ref}}\right) & V_2 < V_{S30} \leq V_u \\ c\ln\left(\frac{V_2}{V_{ref}}\right) - \left[c\ln\left(\frac{V_2}{V_{ref}}\right) + F_{760}\right]\left[\frac{\ln\left(\frac{V_{S30}}{V_u}\right)}{\ln\left(\frac{3000}{V_u}\right)}\right] & V_u < V_{S30} \leq 3000 \text{ m/s} \end{cases} \tag{3}$$

The model form is shown in Figure 3. Term c represents the slope in log–log space for the central portion between corner velocities V_1 and V_2. Velocities V_ℓ and V_u represent the approximate lower and upper limits of the range constrained by observations (200 and

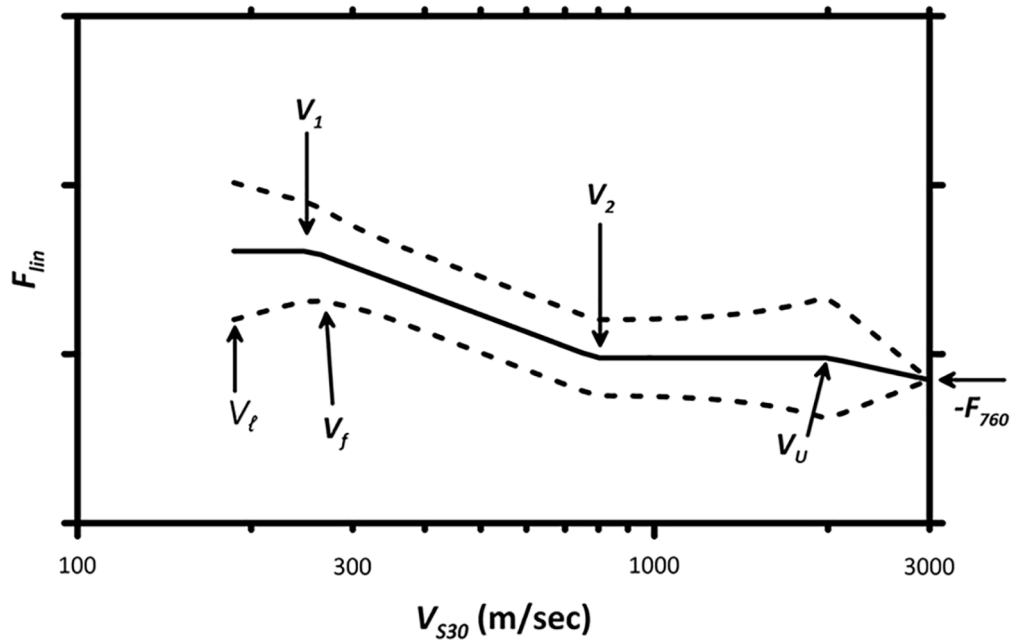

Figure 3. Form of recommended median V_{S30}-scaling model (Equation 3) and the associated uncertainty (Equation 4) for 1.0 s oscillator period.
Coefficients are given in electronic supplement.

2000 m/s, respectively). Velocity V_{ref} is taken as 760 m/s; its physical meaning is the velocity at which $F_V = 0$. The model is flat (constant F_V) for the first and third terms. The last interval of the model represents interpolation between constrained amplification levels at V_u and 3000 m/s, the latter being $-F_{760}$ as shown in Figure 3. Model coefficients c, V_1, and V_2 depend on oscillator period. The coefficients are plotted as a function of period in Figure 4 and are tabulated in the electronic supplement. The basis for the proposed V_{S30}-scaling model is described in the "F_V model development" section below.

The epistemic uncertainty associated with the median model, derived based on panel judgment to capture the range in the median V_{S30}-scaling models considered, is given by a log-normal standard deviation σ_v that is constant over the middle portion of the V_{S30} range (between V_f and V_2) and increases at the low- and high-velocity limits of the model, as shown in Figure 3:

$$\sigma_v = \begin{cases} \sigma_\ell - 2(\sigma_\ell - \sigma_{vc})\frac{V_{S30}-V_\ell}{V_f-V_\ell} + (\sigma_\ell - \sigma_{vc})\left(\frac{V_{S30}-V_\ell}{V_f-V_\ell}\right)^2 & V_\ell < V_{S30} < V_f \\ \sigma_{vc} & V_f \leq V_{S30} \leq V_2 \\ \sigma_{vc} + (\sigma_u - \sigma_{vc})\left(\frac{V_{S30}-V_2}{V_u-V_2}\right)^2 & V_2 < V_{S30} < V_u \\ \sigma_u\left(1 - \frac{\ln\left(\frac{V_{S30}}{V_u}\right)}{\ln\left(\frac{3000}{V_u}\right)}\right) & V_u < V_{S30} < 3000 \text{ m/s} \end{cases} \quad (4)$$

The coefficients for the uncertainty model represent the uncertainty in the central portion of the velocity range (σ_{vc}), the increased uncertainty ($\sigma_\ell - \sigma_{vc}$) at the lower-limit

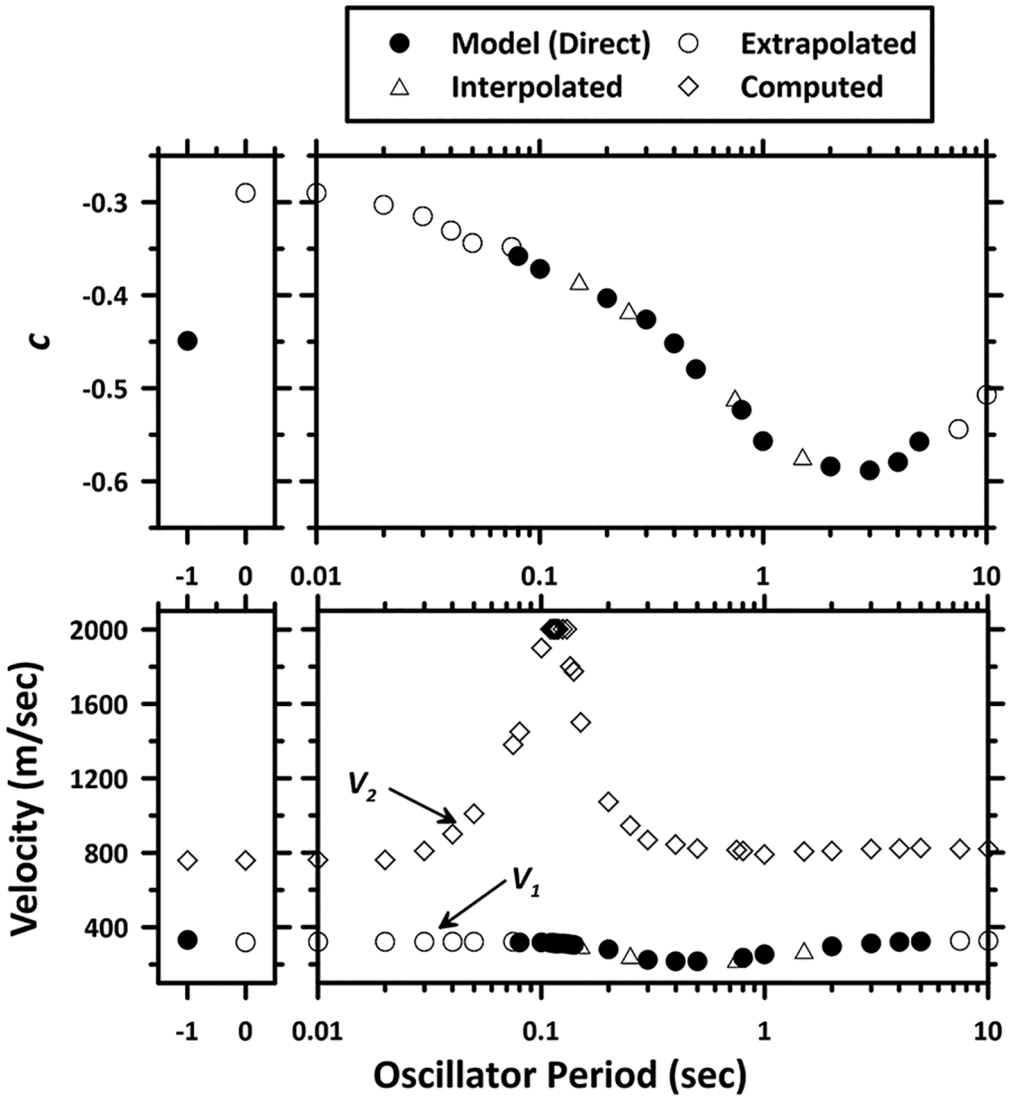

Figure 4. Period-dependence of coefficients in F_V model.
Coefficients that are interpolated, extrapolated, and computed using simulations as a guide are indicated separately from those developed from data and model inferences. In the left plot, 0 indicates PGA and −1 indicates PGV.

velocity for the model (V_ℓ), and the increased uncertainty ($\sigma_u - \sigma_{vc}$) at the upper-limit velocity (V_u). Velocity V_f is specific to the uncertainty model, and velocities V_2 and V_u are the same as for the median model. These and other coefficients are given in the electronic supplement. Details on how the epistemic uncertainty term was developed are given in the "Model uncertainty" section. We do not present an aleatory variability model, which is discussed elsewhere (Goulet et al., 2017; Stewart et al., 2019).

F_{760} model

The F_{760} model modifies ground motion intensity measures from the reference condition of $V_S = 3000$ m/s to $V_{S30} = 760$ m/s as a function of oscillator period. The recommended

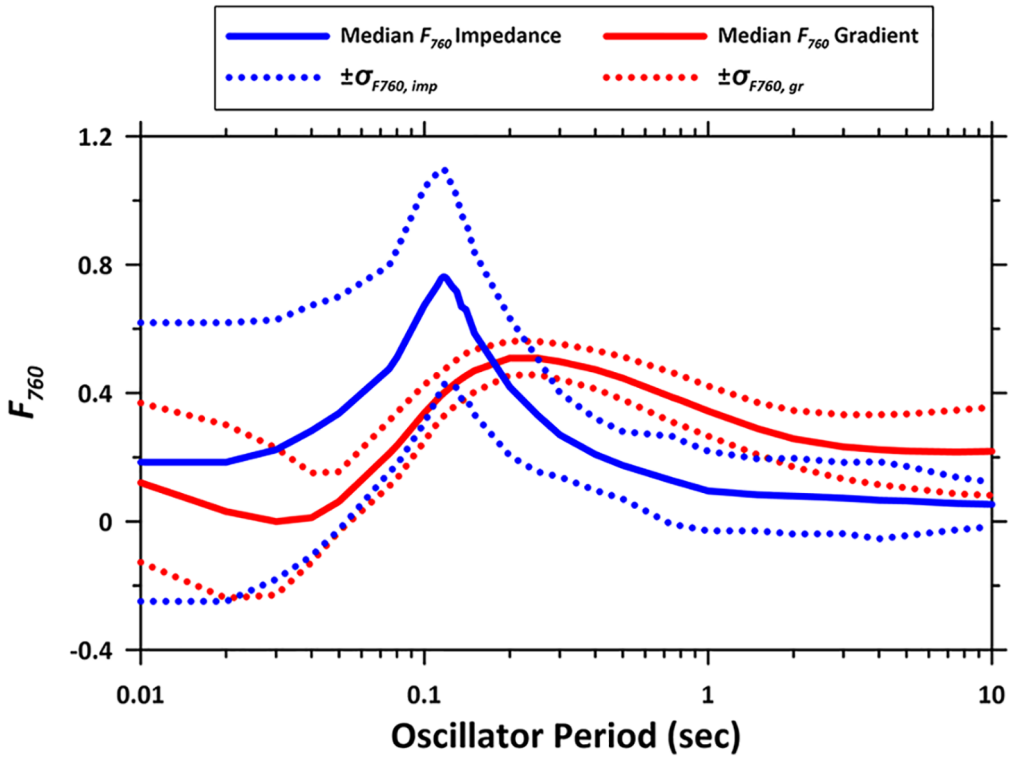

Figure 5. Reference condition site factors, F_{760}, for impedance and gradient conditions and the associated uncertainties as a function of oscillator period.

model is a weighted combination of two models derived from simulations using different groups of velocity profiles (each with V_{S30} = 760 m/s) characterized by (1) large impedance contrasts and (2) relatively gradual velocity gradients. The resulting amplification models are denoted F_{760}^{imp} and F_{760}^{gr}, respectively. Figure 5 shows the median models and their epistemic uncertainties, $\sigma_{\ln F760}$.

The recommended model for F_{760} is given as follows:

$$F_{760}(V_{S30}, T) = w_{imp}(V_{S30})F_{760}^{imp}(T) + w_{gr}(V_{S30})F_{760}^{gr}(T) \tag{5}$$

The weights are a function of V_{S30}. Sites with $V_{S30} \geq V_{w1}$ receive a high weight (w_{imp}) for the F_{760}^{imp} model, and sites with $V_{S30} < V_{w2}$ receive a high weight (w_{gr}) for the F_{760}^{gr} model. The weights taper between the models for velocities between V_{w1} and V_{w2}:

$$w_{imp}(V_{S30}) = \begin{cases} w_1 & \text{for } V_{S30} \geq V_{w1} \\ (w_1 - w_2)\dfrac{\ln\left(\frac{V_{S30}}{V_{w2}}\right)}{\ln\left(\frac{V_{w1}}{V_{w2}}\right)} + w_2 & \text{for } V_{w2} \leq V_{S30} < V_{w1} \\ w_2 & \text{for } V_{S30} < V_{w2} \end{cases} \tag{6}$$

$$w_{gr} = 1 - w_{imp} \tag{7}$$

At each value of V_{S30}, weights w_{imp} and w_{gr} sum to 1.0. Coefficients tabulated in the electronic supplement include the median models (F_{760}^{imp} and F_{760}^{gr}), standard deviations $\sigma_{\ln F760}$, weight transition velocities V_{w1} and V_{w2}, and weights w_1 and w_2. Justification for the proposed model is given in the "F_{760} model development" section.

F_V model development

Models considered

The proposed model for V_{S30}-scaling (F_V) is derived from results of prior research. Here, we describe how results for selected models were adapted for the model-to-model comparisons and explain why certain models were not selected.

We consider two empirical models: (1) a model relating site amplification to peak frequency (f_{peak}) from horizontal-to-vertical spectral ratios (HVSRs) using NGA-East data for CENA (Hassani and Atkinson, 2016b) and (2) an empirical V_{S30}-scaling model developed by the NGA-East Geotechnical Working Group (referred to subsequently as GWG-E; Parker et al., 2019). Additional empirical models that were considered but ultimately not used are Hollenback et al. (2015), Al Noman and Cramer (2015), and Graizer (2015). The site effects model for two Hollenback et al. (2015) GMMs was developed in Fourier amplitude space, which is not readily applicable to response spectral ratios. The GMMs developed by Al Noman and Cramer (2015) and Graizer (2015) were not considered ready to be used as seed models over a wide frequency range (Goulet, personal communication, 2017) and hence were not used here. Upon the completion of the panel's analysis work, a new model was published (Hassani and Atkinson, 2018). Although the principal emphasis of that model was to show the effectiveness of site frequency as a site parameter (building on the work of Hassani and Atkinson, 2016b), they also developed a model based on V_{S30} only. Because the V_{S30}-scaling in that model is similar to GWG-E, a renewal of panel activity to formally consider the Hassani and Atkinson (2018) model was considered unnecessary.

The Hassani and Atkinson (2016b) model provides a representation of amplification that is peaked at site peak frequency f_{peak} (i.e, amplification tapers down for frequencies lower and higher than f_{peak}). To apply this model, we convert V_{S30} to f_{peak} using a relationship between these site parameters as given by Hassani and Atkinson (2016a). Values of f_{peak} corresponding to four values of V_{S30} (one in each NEHRP category D–A) were derived as follows: 270 m/s—2.33 Hz, 560 m/s—7.41 Hz, 1170 m/s—23.8 Hz, and 2032 m/s—57.3 Hz. Tabulated amplification values (provided by B Hassani, personal communication, 2016) were then used to estimate the site term for each approximate V_{S30}. The Hassani and Atkinson (2016b) site amplifications derived from this process are not referenced to the same site condition as the other models (i.e. the site amplification is not zero in ln units at 760 m/s). This was corrected by subtracting the average amplification for Classes C and B (which is the amplification at 760 m/s) from the amplification for each other class. The GWG-E model was used without modification.

Both empirical models use the NGA-East database (Goulet et al., 2014) in their derivation and are based on data with $\mathbf{M} > 3$ and distances $< \sim$600 km. The models used here were developed under the assumption that observed site responses are linear and

effectively independent of magnitude and distance. Recent work has challenged that assumption for studies of response spectra amplification at short oscillator periods, particularly for $\mathbf{M} < 4$ earthquakes (Stafford et al., 2017). Future model refinements to account for such effects are possible, but because the preponderance of the data is for $\mathbf{M} > 4$ events, the linear models are considered applicable for seismic hazard applications in which controlling magnitudes are well above **M** 4.

We also considered four simulation-based models, as introduced in the "Prior work" section: (1) Darragh et al. (2015) (also referred to as Pacific Engineering and Analysis (PEA)), (2) a simulation-based V_{S30}-scaling model developed by the NGA-East Geotechnical Working Group (referred to subsequently as GWG-S; Harmon et al., 2019b), (3) Hwang et al. (1997), and (4) Aboye et al. (2015). The PEA model uses a reference condition of V_S = 3000 m/s. To apply this model, we adjusted amplification values to a reference condition of V_{S30} = 760 m/s by subtracting F_{760} values given in Darragh et al. (2015). Those F_{760} values are based on three different V_S profiles for V_{S30} = 760 m/s sites (denoted gradient, till, and saprolite). As a result, there are three sets of PEA amplification values. Hwang et al. (1997) present tabulated amplification values for 0.2 and 1.0 s PSA for NEHRP categories A–D, which we plot at category mid-velocities (V_{S30} = 1868, 1052, 498, and 243 m/s). The Hwang et al. (1997) results were adjusted to an amplification of 1.0 at V_{S30} = 760 m/s; original results were at 1.0 for Class B. We applied the median model from Aboye et al. (2015) as published (shown in Figure 2 for 1.0 s PSA and Figure E2 of the electronic supplement for 0.2 s PSA). The GWG-S model was provided by J Harmon (personal communication, 2016) in a form that was already referenced to the 760 m/s rock condition by subtracting an F_{760} term provided in Harmon et al. (2019b).

Model comparisons and recommended median model

Figure 6 (for periods of 0.1 and 1.0 s) and the electronic supplement (for PGV and oscillator periods of 0.08, 0.2, 0.3, 0.4, 0.5, 0.8, 2.0, 3.0, 4.0, and 5.0 s) present the considered CENA site amplification models. The models are overlain on inferred site amplifications from observations, which are taken as the mean for each site of within-event rock residuals from Parker et al. (2019). Also shown for comparison is the Seyhan and Stewart (2014) model for active tectonic regions (denoted SS14) and the site factors in the NEHRP provisions for periods of 0.2 and 1.0 s.

One notable feature of the models is that the GWG-S and Aboye et al. (2015) simulation-based models have downward curvature in the V_{S30}-scaling at short periods ($T \leqslant 0.3$ s), which is not present in the PEA model (for the Aboye et al. model, this feature is shown in Figure E2 in the electronic supplement). The difference in simulation results is a consequence of different small-strain soil damping formulations; the physics of wave propagation requires increased damping to decrease ground motion, particularly at high frequencies. The PEA model is based on equivalent-linear simulations that used strain-dependent "Peninsular Range" modulus reduction and damping curves (Silva et al., 1997) as well as a subset of the Electrical Power Research Institute (EPRI) (1993) curves in the upper 150 m with visco-elastic soil below. At greater depths, Darragh et al. (2015) limit the visco-elastic damping such that the site decay parameter (κ_0) did not exceed 0.04 s. The linear visco-elastic simulations in Harmon et al. (2019a) used the small-strain damping ratio (D_{min}) from Campbell (2009) Q-V_S Model 1 without constraining it according to the resulting surface κ_0. As a result, the GWG-S simulations often have higher levels

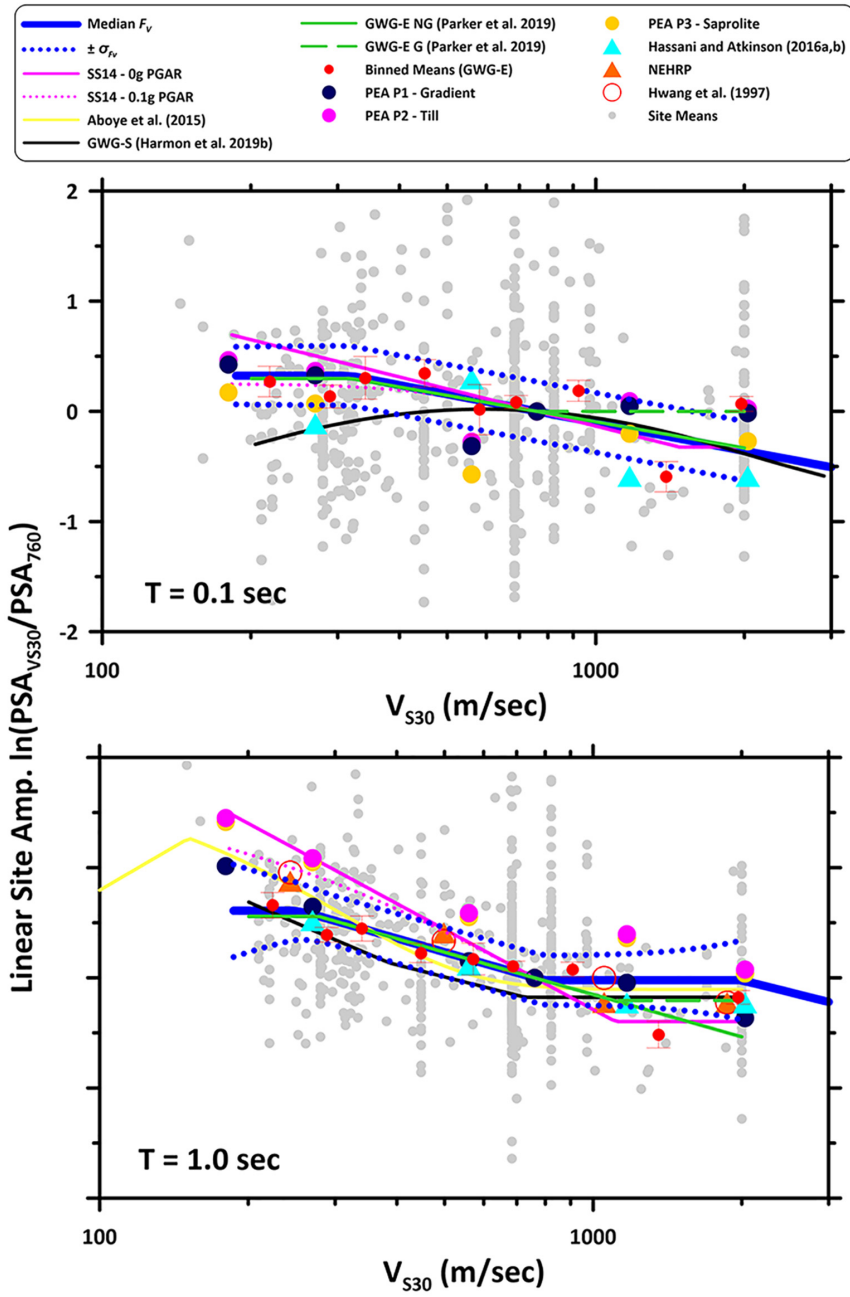

Figure 6. Scaling of site amplification with V_{S30} at oscillator periods of 0.1 and 1.0 s, for CENA region from alternate models, and for a reference model for active tectonic regions.
SS14: Seyhan and Stewart (2014) for active regions, for PGA_r = 0 (linear site amplification only) and for PGA_r = 0.1*g* (as used for developing current NEHRP site factors). GWG-E G and GWG-E NG: Geotechnical Working Group empirically based model for glaciated and nonglaciated regions, respectively (Parker et al., 2019). GWG-S: Geotechnical Working Group simulation-based model (Harmon et al., 2019b). Hassani and Atkinson (2016a, 2016b): f_{peak}-based model for CENA adjusted to unity at 760 m/s. PEA: Darragh et al. (2015) simulation-based model, adjusted to a reference condition of 760 m/s using three simulation-based factors for representative V_S profiles (Profile 1—Gradient, Profile 2—Till, and Profile 3—Piedmont Region Saprolite). Means of within-event rock residuals for each site (i.e. "Site Means"), and their binned means for ranges of V_{S30}, represent the empirical data considered in GWG-E.

of profile damping than those of PEA. The panel elected to not incorporate the downward curvature feature in V_{S30}-scaling into the recommended median model, due to this feature not being evident in the GWG-E empirical data.

The Hassani and Atkinson (2016b) model exhibits peaked behavior in amplification-V_{S30} space at the V_{S30} value corresponding to the PSA oscillator period being plotted. For example, in Figure 6 (oscillator response for $T = 0.1$ s, corresponding to $f_{\text{peak}} = 10$ Hz), the model peaks at ~600 m/s. This behavior is a consequence of f_{peak} being the sole site parameter in the Hassani and Atkinson (2016b) model; in the implementation of the model for this study, V_{S30} is used as a substitute for f_{peak}. Stiffer sites (higher V_{S30}) have higher peak frequencies.

The GWG-E model demonstrates relatively flat scaling at both slow ($V_{S30} < V_1$) and fast ($V_{S30} > V_2$) velocities. Both trends are generally supported by the simulation-based models and have different physical explanations. At slow V_{S30} and short periods, the reduction of scaling is likely due, at least in part, to the effects of soil damping. For longer periods, the cause of the flat scaling at slow V_{S30}, especially as compared to western models (SS14), may be attributable to averaging the effects of peaked response curves over profiles with different average soil depths, which peak near different periods. While sediment depth information at seismograph sites is generally unknown, Parker et al. (2019) investigated bias in the GWG-E model for sites in particular sedimentary basins, where depths are expected to be greater than for non-basin sites. They found no systematic differences between basin and non-basin sites. The best agreement between GWG-E and simulation-based models is at $V_{S30} > \sim 400$ m/s and $T > 0.2$ s.

The model for active tectonic regions (SS14) provides a poor match to the CENA results for most periods. Some particular areas of divergence are as follows:

- The SS14 model does not flatten the V_{S30}-scaling at slow velocities.
- For the central range of V_{S30} (approximately between V_1 and V_2), the SS14 V_{S30}-scaling is steeper than that for CENA models, especially at long periods.

Because the NEHRP site factors follow the SS14 model, just as the CENA results reject SS14, they also reject the current NEHRP factors.

The panel based the median model largely on GWG-E. Referring to Equation 3, the zero gradient for $V_\ell < V_{S30} < V_1$ and slope c for $V_1 < V_{S30} < V_2$ are taken from GWG-E. The third and fourth elements of the recommended model (i.e. the segments for $V_{S30} > V_2$) were constrained by simulations as described further below in the "Fast velocity model elements" section. A second exception is that at slow velocities and oscillator periods of 0.3–0.8 s, we decrease V_1 from GWG-E values, which raises the amplification. This change was motivated by the GWG-E amplification being lower than that for other models for soft soils in this period range.

Period interpolation and extrapolation

The original work of the panel was constrained by the useable period range of NGA-East data, which is approximately 0.08–5.0 s. At the request of USGS, the panel estimated coefficients for a wider range of periods and for a few periods inside of the originally considered range but for which plots such as in Figure 6 and the electronic supplement had not been developed. Intensity measures for which these estimates are provided are indicated in Figure 4 (both interpolated and extrapolated). Parameter V_2 is not obtained by

interpolation or extrapolation, but rather by procedures described in the next section. Interpolated periods are 0.15, 0.25, 0.75, and 1.5 s. Coefficients other than V_2 in Equations 3 and 4 were obtained by log-linear interpolation of the nearest neighbors.

In the case of extrapolated short period coefficients (0.01, 0.02, 0.03, 0.04, 0.05, and 0.075 s), we considered the trend of coefficients with period as provided by simulations (Harmon et al., 2019a, 2019b). In the simulation results, coefficient c increases modestly for periods less than 0.1 s to a local peak at 0.015 s and then saturates to match the values for PGA at about 0.007 s. These features are shown in Figure 4 (the peak at 0.015 sec is not shown because coefficients are not provided at this period). We use a target value of c at the 0.015 s peak that is 20% larger (i.e. less negative) than that at 0.1 s (–0.28), which is motivated by this same shift in simulation-based coefficients. For V_1, values derived from data increase as the period shortens (Figure 4) toward 0.1 s, which is consistent with features in the simulation-based model. Simulation-based values of V_1 saturate for periods under about 0.1 s; we follow this pattern, using the V_1 at 0.1 s for shorter periods.

In the case of extrapolated long period coefficients (7.5 and 10 s), we project values of c using the slope computed between existing coefficients at 4.0 and 5.0 s (Figure 4). This pattern matches the general trend of models for active regions. We prefer the use of empirical model trends to guide our extrapolation here rather than simulation results due to difficulties in modeling site response with 1D GRA at long periods (e.g. Stewart et al., 2017a). For V_1, we maintain the value at 5.0 s for longer periods.

Fast velocity model elements

The empirical data in Figure 6 provide relatively weak constraint to the F_V model for fast sites ($V_{S30} > 1000$ m/s). To provide guidance on site amplification in this range, we examined simulation results for sites with $V_{S30} = 2000$ m/s by Boore (2015). Boore (2015) performed computations using the square-root-impedance method, also known as the quarter-wavelength method. These simulations used velocity profiles with $V_{S30} = 2000$ and 3000 m/s, which were modified from the very hard rock crustal model of Boore and Joyner (1997). The site damping parameter κ_0 was taken as 0.006 s for both profiles, which is generally consistent with a recent data compilation by Xu et al. (this issue). Figure 7 shows the site amplification at 2000 m/s relative to the 3000 m/s reference as interpreted from these simulations. The simulation results in Figure 7 are not uniformly distributed within the shown range; for the magnitude–distance combinations most likely to control hazard, results are concentrated near the upper end of the range, which motivated our setting of the target amplification shown in Figure 7.

The target values of site amplification at 2000 m/s, shown in Figure 7, were used to constrain the F_V model (i.e. the model predictions at $V_{S30} = 2000$ m/s match target values). The F_V values were computed from the target results in Figure 7 as follows:

$$F_V(V_u) = \ln(Y_{2000}) - F_{760}^{imp} \tag{8}$$

where V_u is 2000 m/s and Y_{2000} is the target site amplification in Figure 7. We used the impedance model for F_{760} in this case, which we consider to be more appropriate for fast sites. The model in Equation 3 is formulated to provide an amplification of $F_V(V_u)$ for $V_2 < V_{S30} < V_u$. We obtain this by adjusting V_2 from the original GWG-E values to match F_V to the target amplification. The adjusted values of V_2 are shown in Figure 4

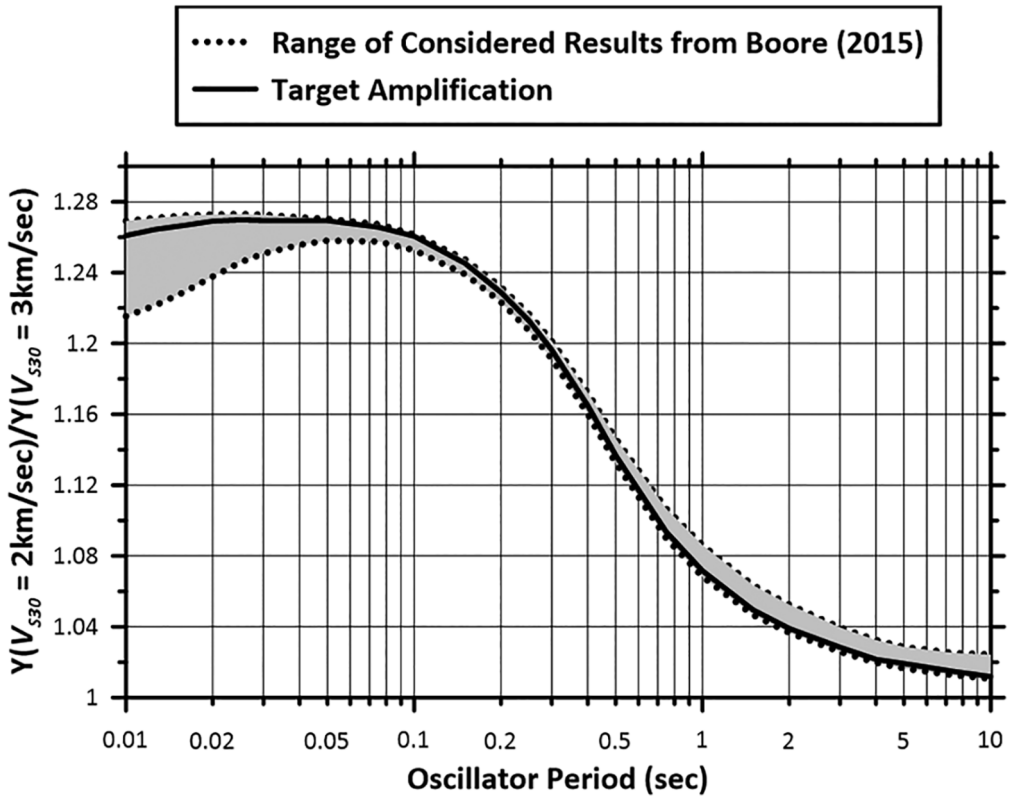

Figure 7. Simulation-based site amplification for V_{S30} = 2000 m/s site relative to 3000 m/s reference condition, derived from Boore (2015).
The range represents results from input ground motions for **M** = 6–8 events and R_{RUP} = 10–100 km.

(labeled as Computed). The last line of Equation 3 provides for a linear decrease in amplification from $F_V(V_u)$ to $-F_{760}$ between V_u and 3000 m/s.

Model uncertainty

The F_V model epistemic uncertainty, as given in Equation 4 with coefficients in the electronic supplement, is shown in Figure 6 and in the electronic supplement. This epistemic uncertainty applies to the median model and would typically be implemented in probabilistic seismic hazard analysis (PSHA) through the use of logic trees (e.g. Bommer et al., 2005; McGuire, 2004). Aleatory variability of the site amplification (ϕ_{S2S}) was not evaluated by this panel; further information on aleatory variability in CENA site amplification is given by Goulet et al. (2017) and Stewart et al. (2019).

The epistemic uncertainty model was developed using expert judgment, rather than through a formal calculation of standard deviations between models. This approach was applied for three principal reasons: (1) the variations among models is uneven across periods, being relatively low for $T > 1$ s and larger at shorter periods; in the judgment of the panel, these period-to-period features do not reflect true epistemic uncertainties in site amplification; (2) for many periods, the recommended median model is not at the center of the range of the various models in log space (there are often more models above than below the median)—as

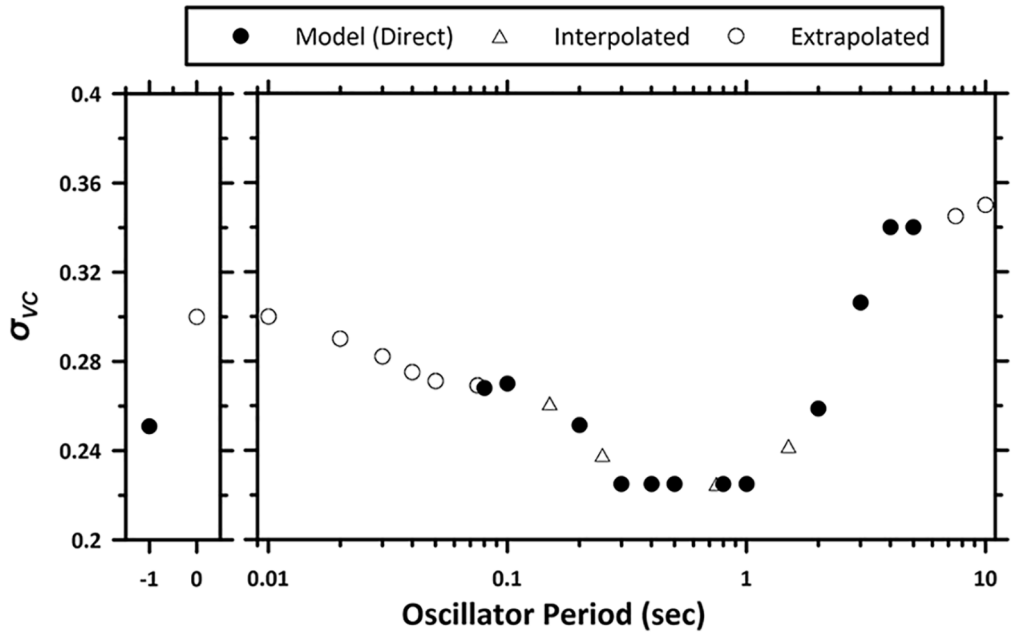

Figure 8. Trend with period of epistemic uncertainty parameter σ_{vc} as developed from observation and as extrapolated to short and long periods.

a result, application of a formal standard deviation around the median model would not have encompassed the alternative models; and (3) the panel judged that increases in the model uncertainty should be applied at upper and lower ends of the velocity range, where data are sparse; reliance on common statistical methods would not necessarily provide this.

Based on visual inspection of the distribution of models, we proposed a range intended to represent ± 1 standard deviation (σ_v). We centered the model on the median, to have the width of the range represent uncertainty in a smoothly varying manner across the velocity range. In Equation 4, σ_{vc} represents standard deviation in the central portion of the velocity range, which is plotted as a function of period in Figure 8. The relations in Equation 4 for $V_\ell < V_{S30} < V_1$ and $V_u > V_{S30} > V_2$ are second-order polynomials constrained to have a value of σ_{vc} and zero slope at V_1 and V_2.

As shown in Figure 3, the uncertainty decreases linearly toward zero between V_u and 3000 m/s. This is applied because the epistemic uncertainty for sites at or near 3000 m/s is captured by the NGA-East GMMs (Goulet et al., 2018), and further uncertainty associated with site amplification is unnecessary.

We increased model uncertainty at short and long periods where coefficients were extrapolated. Figure 8 shows these increases to σ_{vc} beyond the observation range of 0.08–5.0 s. Similar increases are provided for σ_ℓ and σ_u. These increases were largely based on expert judgment. Values of V_f were also increased in the extrapolation region, which has the effect of broadening the velocity range with increased uncertainty (i.e. lines 1 and 3 in Equation 4).

F_{760} model development

Models considered

The proposed model for adjusting ground motion intensity measures from the V_S = 3000 m/s reference condition to V_{S30} = 760 m/s (F_{760}) is based on alternative GRAs. This section presents the considered simulation results.

The panel considered results from four investigations—Boore and Campbell (2017), PEA, GWG-S, and Frankel et al. (1996) (later applied in Atkinson and Boore, 2006). Boore and Campbell (2017) use both a square-root impedance approach and an approach that captures site resonance effects. We consider the Boore and Campbell (2017) results to largely supersede results from previous related studies (Beresnev and Atkinson, 1997; Boore, 2015; Boore and Joyner, 1997; Boore and Thompson, 2015). PEA used random vibration theory–based equivalent-linear GRAs that captured resonance and nonlinear effects. GWG-S used linear visco-elastic GRAs that captured resonance effects. Different material damping models were used in these studies, as discussed previously. The Frankel et al. (1996) study was re-done here using a square-root impedance approach.

Figure 9 shows the profiles used by PEA, Frankel et al. (1996), and a representative selection of those used in GWG-S. The GWG-S profiles are based on measurements from CENA sites for which V_{S30} is between 700 and 800 m/s. The Boore and Campbell (2017) profiles (not shown in Figure 9) are similarly selected to be within 10% of 760 m/s and as a group are qualitatively similar to those of GWG-S. The three PEA profiles are intended to be representative of three different CENA geologic conditions: glacial till, Piedmont saprolite, and a weathered rock gradient, all with V_{S30} = 760 m/s. They were constructed using suites of measured profiles reflecting these near-surface geologic conditions. The Frankel et al. (1996) profile represents a rather gradual increase in velocity with depth. A typical feature of the profiles considered by Boore and Campbell, PEA (till, saprolite), and GWG-S is the presence of impedance contrasts; these profiles were used to develop the impedance model (F_{760}^{imp}). The weathered rock (PEA) and gradient (Frankel et al.) profiles lack large impedance contrasts; these were used to develop the gradient model (F_{760}^{gr}).

Aside from V_S profiles, the other site parameter that strongly influences F_{760} is the site damping parameter κ_0. Based on an assessment by Boore and Campbell (2017), we use their simulation results for κ_0 = 0.01, 0.02, and 0.03 s. PEA uses κ_0 = 0.02 s for 760 m/s profiles. The re-working of the Frankel et al. (1996) analyses that was performed here used site κ_0 = 0.01 and 0.02 s. The GWG-S simulations employ a material damping model, which does not require specification of κ_0.

Amplifications of Fourier spectra can be computed using only V_S profiles and site damping, but to convert these to ratios of response spectra requires simulations of ground motion intensity measures for various magnitudes and distances. These simulations usually use the point-source stochastic (e.g. Boore, 2003) or similar methods. To encompass a range of conditions, we took results from Boore and Campbell for **M** 5 at 10 km and **M** 8 at 500 km. The utilized PEA amplification results are conditioned on rock PGA in lieu of magnitude and distance (ranges given in "Prior work" section). The GWG-S input motions are for hard rock site conditions (V_S = 3000 m/s) and are rich in high-frequency energy. Harmon et al. (2019b) have F_{760} models for a variety of depths to the 3000 m/s shear-wave horizon; the results presented here represent an average over the considered depth range. The Fea96 gradient profile in Figure 9 was re-analyzed using input motions for **M** 4.5 and 6.5 and rupture distances of 10, 50, and 100 km.

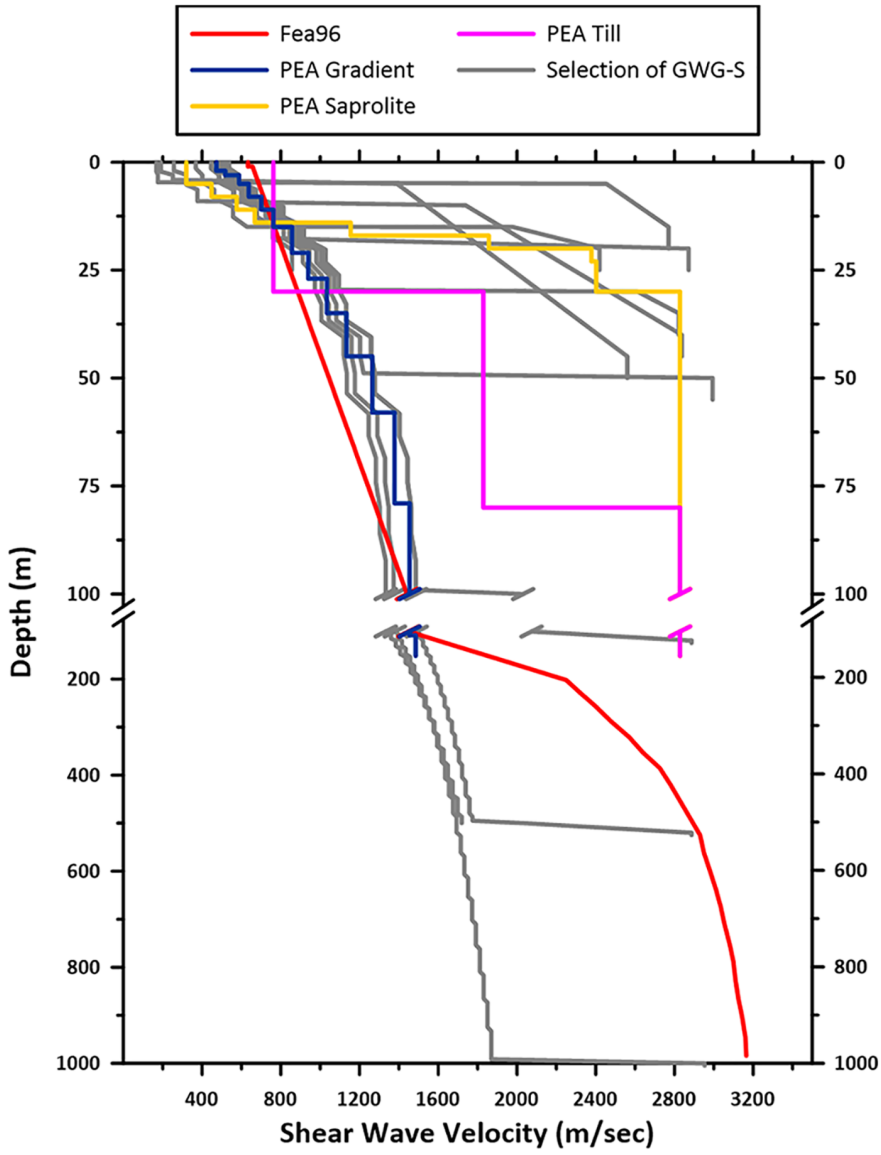

Figure 9. Shear-wave velocity versus depth profiles in CENA with V_{S30} between 700 and 800 m/s (marked as GWG-S in legend; Harmon et al., 2019a) or equivalent to 760 m/s as given by PEA (Piedmont saprolite, till, weathered firm rock) and Frankel et al. (1996) (gradient).

Recommended impedance and gradient models

Figure 10 shows the resulting PSA ratios from the three sets of simulations for impedance conditions. Most of the results have a similar shape, with a peak near 0.1–0.2 s, decay toward no amplification (unity) at long periods, and highly variable behavior at periods below the peak as a result of model-to-model variability and different κ_0 values. We consider all of the results in Figure 10 to be credible representations of F_{760} behavior for impedance conditions. Accordingly, the recommended model is the median of the models

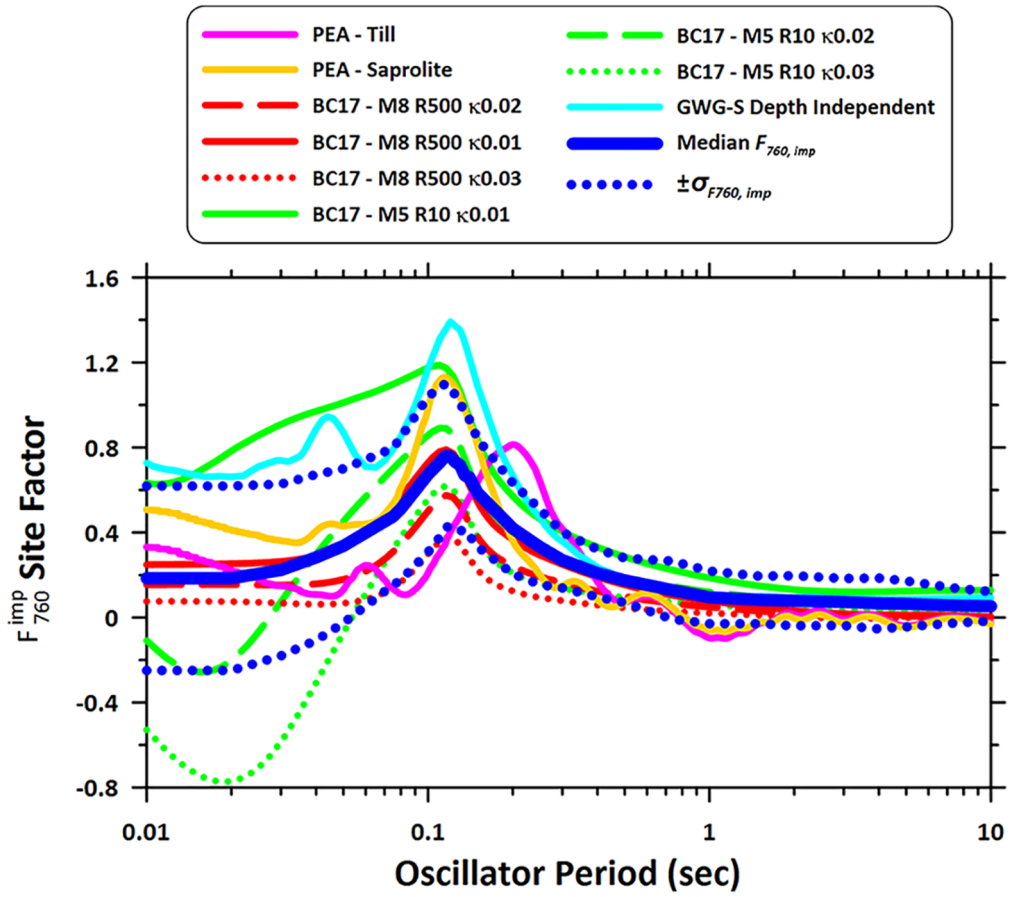

Figure 10. Reference site factor F_{760} for impedance profiles from Boore and Campbell (2017) (labeled BC17), PEA (Darragh et al., 2015), and GWG-S (Harmon et al., 2019b).

shown in the figure. The uncertainty shown in the figure ($\sigma_{\ln F760}$) represents a smoothed standard deviation between models, which decreases appreciably with period.

Figure 11 shows amplification results for gradient conditions. The gradient amplifications lack the peak near 0.1 s and tend to have larger amplification for $T > 0.2$ s. The median model and uncertainty encompass the available models, with the exception of results for $\kappa_0 = 0.01$ s at short periods.

Model weights

The impedance and gradient F_{760} models have distinct features, and for many applications, guidance is needed on when to select the impedance versus the gradient F_{760} model to pair with F_V. As shown in Figure 5, the differences between F_{760} models are appreciable.

For applications in which a V_S profile is available for bedrock materials below any soil layers, and this profile extends far enough into the bedrock to characterize V_S within and below the weathered zone, F_{760} model selection should be based on profile attributes. The impedance model is preferred when the portion of the profile in rock- or rock-like

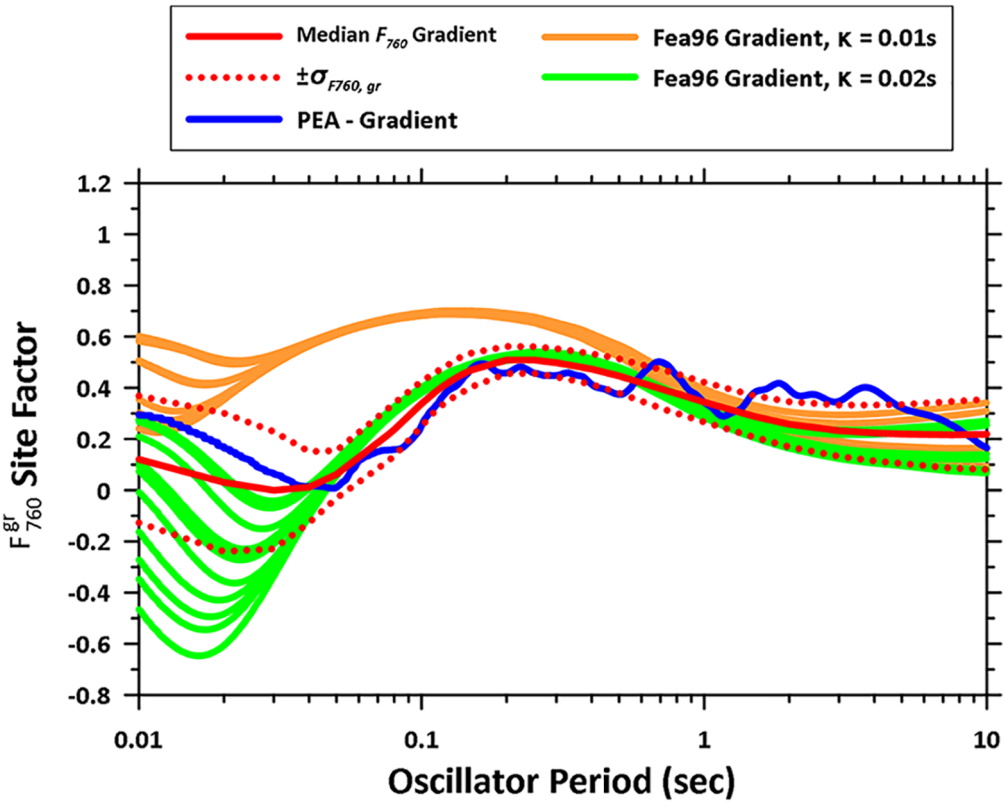

Figure 11. Reference site factor F_{760} for gradient profiles from PEA (Darragh et al., 2015) and Frankel et al. (1996), as re-analyzed in this study (labeled Fea96).

materials includes an appreciable impedance contrast. The gradient model is preferred when rock materials exhibit a more gradual increase in velocity with depth.

For many applications, a site *Vs* profile that extends through the weathered zone of bedrock materials is not available. For such applications, we recommend to use a weighted average of the two F_{760} models based on the V_{S30} at the site (Equation 5). The panel anticipated that impedance conditions would be more prevalent at sites with high V_{S30} and that gradient conditions would be more common at sites with low V_{S30}. To investigate the degree to which this hypothesis is correct and to guide the selection of appropriate model weights, we examined spectral shapes from CENA ground motions for different V_{S30} ranges.

After binning by earthquake magnitude (**M**), rupture distance (R_{RUP}), and V_{S30}, the available spectra were normalized by the average PSA between 0.08 and 1.5 s oscillator periods. The spectral shapes for **M** = 4–5.5, R_{RUP} = 0–150 km, and V_{S30} bins around 2000, 760, 500, and 260 m/s are shown in Figure 12. The data show strong peaks in the range of 0.05–0.1 s in the mean spectral shape for recordings at sites with V_{S30} exceeding 500 m/s and a low-amplitude, broad peak between 0.1 and 0.3 s at 260 m/s. While the spectra in Figure 12 include source, path, and site effects, the changes in shape between V_{S30} groups can be attributed mostly to site effects as the average source and path effects

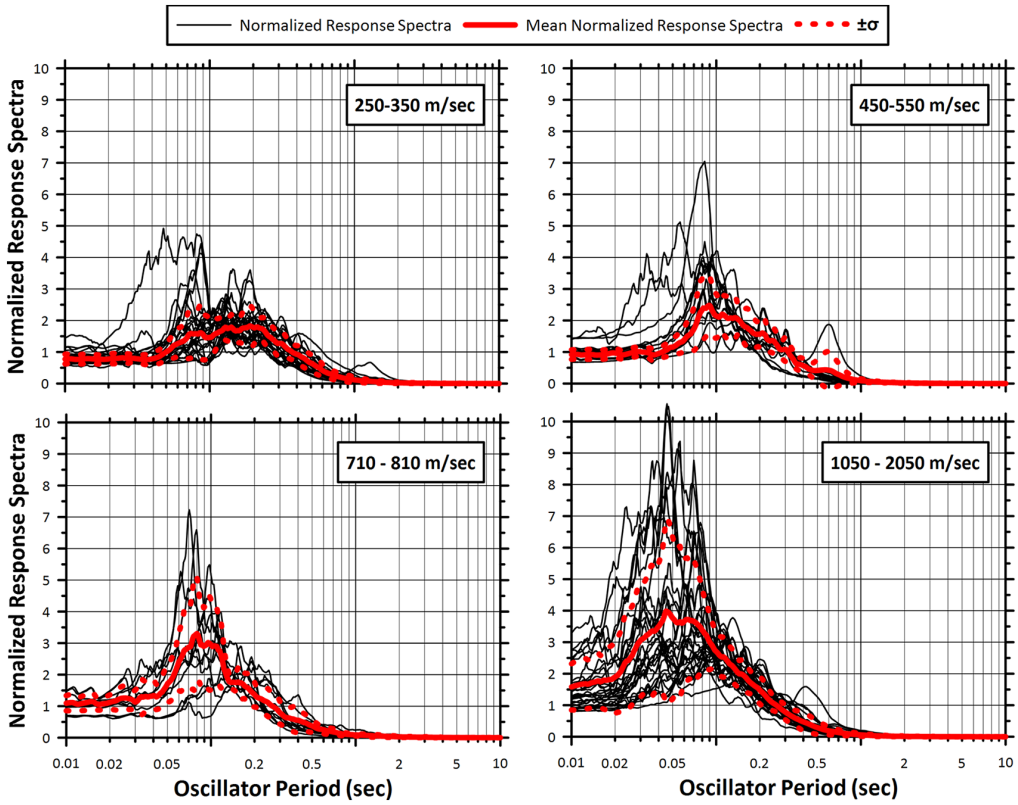

Figure 12. Spectral shapes of NGA-East data for **M** 4–5.5 earthquakes recorded at R_{RUP} between 0 and 150 km at sites within the approximate V_{S30} ranges marked in the figures.
Spectral shapes are normalized by the average response between 0.08 and 1.5 s.

are broadly similar between V_{S30} groups. These trends match those observed by Hassani and Atkinson (2016a) in the NGA-East data, in which the peak of the HVSR is near 0.1 s (10 Hz) for sites with V_{S30} = 500–1000 m/s. Results similar to Figure 12 are also obtained from spectral shapes of simulated motions for different site conditions (J Harmon, personal communication, 2018).

The weighting model in Equations 6 and 7 assigns different weights to the impedance and gradient models for different V_{S30} values. Alternate weight assignments have been discussed among the panel and between the first author (J.P.S.) and USGS technical staff. One approach, preferred by the panel, gives preference to the impedance model for fast sites and to the gradient model for slow sites. Proponents suggested w_1 = 0.9, w_2 = 0.1, V_{w1} = 600 m/s, and V_{w2} = 400 m/s. We also considered a second approach that gives equal weight to impedance and gradient models for fast V_{S30} sites and preference to the gradient model for soft sites. For use in the 2018 national maps, the decision was ultimately made to give 2/3 weight to approach 1 and 1/3 weight to approach 2 for firm sites, resulting in w_1 = 0.767. For soft sites, the gradient model was preferred by consensus, resulting in w_2 = 0.1. The transition velocities are V_{w1} = 600 m/s and V_{w2} = 400 m/s.

Summary and discussion

Summary recommendation

We recommend that ergodic (non-site-specific), linear, V_{S30}-based site amplification (F_{lin}) in CENA be computed using Equations 1 to 3 and 5 to 7, with the coefficients given in the electronic supplement. The corresponding nonlinear term (F_{nl}) is given in Hashash et al. (2017; this issue). The complete model (F_S) has three components in natural log units: F_V for V_{S30}-scaling referenced to V_{S30} = 760 m/s, F_{760} for amplification of the 760 m/s site condition relative to the reference of V_S = 3000 m/s, and F_{nl} for nonlinear effects. These models are based on a combination of ground motion data analysis and GRA simulations. The form of the F_V model is constrained by data, except for very stiff sites where it is constrained by simulations. The F_{760} models are simulation-based, with an impedance model representing conditions with large shallow impedance contrast (applicable to stiff sites) and a gradient model representing conditions with a relatively deep weathering profile and no strong impedance contrasts (applicable to soft sites).

We recognize our recommendations depart substantially from past practice in CENA, which was based on site factors developed for active tectonic regions. NGA-East data and simulations demonstrate that such models are biased for application to CENA sites.

Site responses at many CENA sites are controlled by large impedance contrasts caused by shallow sediments overlying hard rock, often created by glacial scour and subsequent sediment deposition. Such sites can have strong resonance effects, most frequently at short fundamental periods. Because V_{S30} is a depth-averaged velocity with no direct relationship to site frequency, V_{S30}-based site response models like those provided here necessarily smooth across variable site resonances and other effects. Such effects can be better described by models that incorporate information on the site frequency or sediment depth in combination with V_{S30}. We encourage considering these effects as part of site-specific analyses. The use of such models was beyond the scope of this study, but could be considered in future versions of the USGS national seismic hazard maps.

Model performance

The linear amplification resulting from the recommended model is given for various V_{S30} in Figure 13. The amplification is peaked near 0.1 s for velocities up to about 500 m/s, as seen in data. The peak in the amplification then shifts to longer periods for softer sites. Including nonlinear effects (not shown in Figure 13) would further emphasize the shift to longer periods for strong shaking conditions.

Model rationale

Several strategies employed in model development are presented here as answers to frequently-posed questions.

Why did we adopt a hybrid approach in which simulations are solely used for the nonlinear model while empirical data in conjunction with simulations were considered for the linear model? First, there is precedent for combining information sources in a hybrid manner for application in active tectonic regions (e.g. Dobry et al., 2000; Seyhan and Stewart, 2014). Second, ground response simulations can give accurate estimates of nonlinear effects (e.g. Kwok and Stewart, 2006) even if their prediction of absolute levels of site amplification

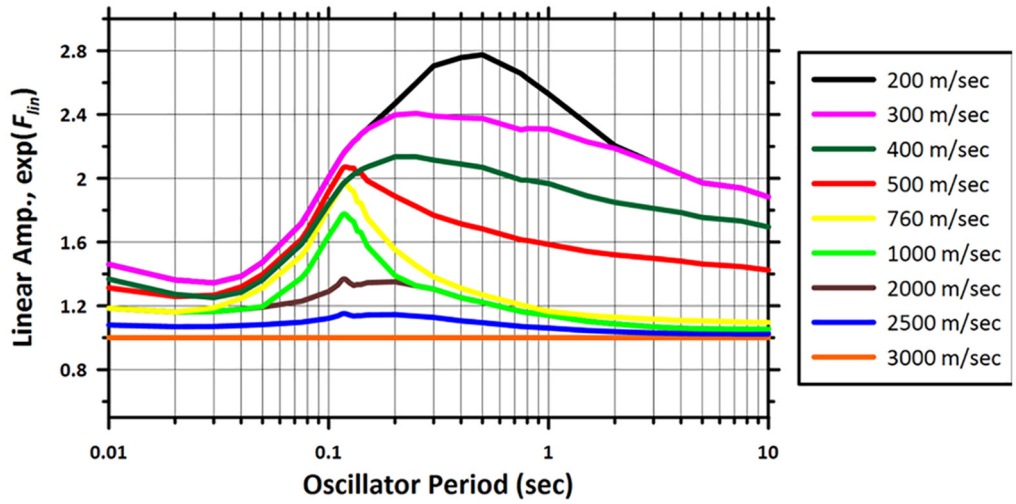

Figure 13. Linear amplification for oscillator periods from 0.01 to 10 s for various V_{S30} using the proposed model with selected weights for USGS maps.

from ground response simulations can be erroneous (e.g. Baturay and Stewart, 2003; Kaklamanos and Bradley, 2018; Thompson et al., 2012).

Why do we split the linear amplification term into two components instead of using a single term referenced to V_S = 3000 m/s? The empirical data are useful to constrain the changes in site amplification over the range of site conditions present in the dataset, which is approximately V_{S30} = 200–2000 m/s. There is no observational basis for extending this range to the 3000 m/s reference condition. As a result, the model discussed here uses data where it exists and uses simulations for the step from 760 to 3000 m/s, which is considered preferable to the alternative of not using data and relying solely on simulations to evaluate site amplification for all V_{S30} relative to 3000 m/s (e.g. as in Boore and Campbell, 2017; Darragh et al., 2015; Harmon et al., 2019a, 2019b).

Limitations

The models presented in this article are considered applicable for evaluating ergodic site response effects for V_{S30} = 200–3000 m/s and intensity measures of PGA, PGV, and PSA for oscillator periods between 0.01 and 10.0 s. Due to sensitivity of response spectral amplification to spectral shape, and the sensitivity of spectral shape to magnitude and distance, the models provided here are considered appropriate for $\mathbf{M} > 4$ earthquakes and site-to-source distances <400 km.

Because they are ergodic, the models presented here do not provide site-specific estimates of site response, even if V_{S30} is measured at the site of interest. As a result, an ergodic standard deviation model should be used (that incorporates site-to-site dispersion, ϕ_{S2S}) when the site terms in this article are applied in combination with a reference rock GMM. Models for ergodic aleatory variability are discussed in Goulet et al. (2017) and Stewart et al. (2019). Additional site condition attributes, such as site frequency, depth to bedrock, or dynamic material properties, could be introduced to improve site response

estimates. Resonance effects are known to be strong at many CENA sites due to soil layers deposited over hard rock, so consideration of these effects can have a substantial impact on site response estimates. Such effects can be considered through the use of empirical models conditioned on these additional parameters (e.g. Hassani and Atkinson, 2016b, 2018), simulation-based models (Harmon et al., 2019b), or the development of site-specific (or non-ergodic) site amplification models.

Finally, we have a recommendation associated with the application of the site response models in this article with NGA-East GMMs. Ideally, the development of GMMs and site terms should occur in a coordinated manner. This can be achieved by considering the site variables directly within the GMM regression framework. In NGA-East, a different approach was used whereby site amplification models were used to correct ground motion intensity measures to a reference site condition, and source and path attributes were then evaluated from regression on the site-corrected data. The coordination referred to above would require that the site models used to correct the data are the same as those used for the forward application. However, that was not the case for CENA with the NGA-East GMMs (Goulet et al., 2017, 2018; PEER, 2015a, 2015b) and the site amplification model provided here. As a result, it is possible that bias will be found when CENA data are compared to NGA-East GMMs combined with our site amplification models. Accordingly, we recommend future work to re-evaluate the NGA-East GMMs using the available data and our site model and that appropriate adjustments (likely to the constant term in the GMMs) be made to remove any bias that might be identified.

Acknowledgments

We thank Mark Petersen, Arthur Frankel, and Peter Powers of the USGS, Yousef Bozorgnia of UCLA, Robert Darragh of Pacific Engineering and Analysis, and Christine Goulet of SCEC for their input and encouragement. Behzad Hassani of Western University (Canada) as well as Joseph Harmon and Okan Ilhan of University of Illinois are thanked for supporting the project by providing digital files related to their research. We also thank three anonymous reviewers and the associate editor for thoughtful feedback that improved the quality of this manuscript. Any opinions, findings, and conclusions or recommendations expressed in this report are those of the authors and do not necessarily reflect the opinions or policy of the USGS.

Declaration of conflicting interests

The author(s) declared no potential conflicts of interest with respect to the research, authorship, and/or publication of this article.

Funding

The author(s) disclosed receipt of the following financial support for the research, authorship, and/or publication of this article: This project was sponsored by US Geological Survey (USGS) contract G16AP00005. This support is gratefully acknowledged.

References

Aboye SA, Andrus RD, Ravichandran N, et al. (2015) Seismic site factors and design response spectra based on conditions in Charleston, South Carolina. *Earthquake Spectra* 31: 723–744.

Al Noman MN and Cramer CH (2015) *Empirical ground-motion prediction equations for eastern North America*. PEER report no. 2015/04. Berkeley, CA: Pacific Earthquake Engineering Research Center, University of California.

Atkinson G and Boore DM (2006) Earthquake ground-motion prediction equations for eastern North America. *Bulletin of the Seismological Society of America* 96: 2181–2205.

Baturay MB and Stewart JP (2003) Uncertainty and bias in ground-motion estimates from ground response analyses. *Bulletin of the Seismological Society of America* 93: 2025–2042.

Beresnev IA and Atkinson GM (1997) Shear-wave velocity survey of seismographic sites in eastern Canada: Calibration of empirical regression method of estimating site response. *Seismological Research Letters* 68: 981–987.

Bommer JJ, Scherbaum F, Bungum H, et al. (2005) On the use of logic trees for ground-motion prediction equations in seismic hazard analysis. *Bulletin of the Seismological Society of America* 95(2): 377–389.

Boore DM (2003) Simulation of ground motion using the stochastic method. *Pure and Applied Geophysics* 160: 635–675.

Boore DM (2013) The uses and limitations of the square-root impedance method for computing site amplification. *Bulletin of the Seismological Society of America* 103: 2356–2368.

Boore DM (2015) *Adjusting ground-motion intensity measures to a reference site for which* $VS30 = 3000$ *m/s*. PEER report no. 2015/06. Berkeley, CA: Pacific Earthquake Engineering Research Center, University of California.

Boore DM and Campbell KW (2017) Adjusting central and eastern North America ground-motion intensity measures between sites with different reference-rock site conditions. *Bulletin of the Seismological Society of America* 107: 132–148.

Boore DM and Joyner WB (1997) Site amplifications for generic rock sites. *Bulletin of the Seismological Society of America* 87: 327–341.

Boore DM and Thompson EM (2015) Revisions to some parameters used in stochastic-method simulations of ground motion. *Bulletin of the Seismological Society of America* 105: 1029–1041.

Building Seismic Safety Council (BSSC) (2018) *Project 17 Committee* (Chair Ronald O. Hamburger). Washington, DC: National Institute of Building Sciences, BSSC.

Campbell KW (2009) Estimates of shear-wave Q and $\kappa 0$ for unconsolidated and semiconsolidated sediments in eastern North America. *Bulletin of the Seismological Society of America*, 99, 2365–2392.

Darragh RB, Abrahamson NA, Silva WJ, et al. (2015) *Development of hard rock ground-motion models for region* 2 *of central and eastern North America*. PEER report no. 2015/04201504. Berkeley, CA: Pacific Earthquake Engineering Research Center, University of California.

Dobry R, Borcherdt RD, Crouse CB, et al. (2000) New site coefficients and site classification system used in recent building seismic code provisions. *Earthquake Spectra* 16: 41–67.

Electrical Power Research Institute (EPRI) (1993) *Guidelines for determining design basis ground motions*. Report no. EPRI TR-102293. Palo Alto, CA: Electrical Power Research Institute.

Frankel AD, Mueller CS, Barnhard T, et al. (1996) *National seismic hazard maps: Documentation*. USGS open-file report no. 96-532. Reston, VA: USGS.

Goulet CA, Bozorgnia Y, Abrahamson NA, et al. (2018) *Central and eastern North America ground—motion characterization—NGA-East final report*. PEER report 2018/08. Berkeley, CA: Pacific Earthquake Engineering Research Center.

Goulet CA, Bozorgnia Y, Kuehn N, et al. (2017) *NGA-East ground-motion models for the U.S. Geological Survey National Seismic Hazard Maps*. PEER report no. 2017/03. Berkeley, CA: Pacific Earthquake Engineering Research Center.

Goulet CA, Kishida T, Ancheta TD, et al. (2014) *PEER NGA-East database*. PEER report no. 2014/17201417. Berkeley, CA: Pacific Earthquake Engineering Research Center.

Graizer V (2015) *Ground-motion prediction equations for the central and eastern United States*. PEER report no. 2015/04. Berkeley, CA: Pacific Earthquake Engineering Research Center, University of California.

Harmon JA, Hashash YMA, Stewart JP, et al. (2019a) Site amplification functions for central and eastern North America—Part I: Simulation dataset development. *Earthquake Spectra* 35: 787–814.

Harmon JA, Hashash YMA, Stewart JP, et al. (2019b) Site amplification functions for central and eastern North America—Part II: Modular simulation-based models. *Earthquake Spectra* 35: 815–847.

Hashash YMA and Park D (2001) Non-linear, one-dimensional seismic ground motion propagation in the Mississippi embayment. *Engineering Geology* 62: 185–206.

Hashash YMA, Harmon JA, Ilhan O, et al. (2017) *Recommendations for ergodic nonlinear site amplification in central and eastern North America*. PEER report 2017/05. Berkeley, CA: Pacific Earthquake Engineering Research Center, University of California.

Hashash YMA, Ilhan O, Harmon JA, et al. (this issue) Nonlinear site amplification model for ergodic seismic hazard analysis in central and eastern North America. *Earthquake Spectra*.

Hashash YMA, Kottke AR, Stewart JP, et al. (2014) Reference rock site condition for central and eastern North America. *Bulletin of the Seismological Society of America* 104: 684–701.

Hashash YMA, Tsai CC, Phillips C, et al. (2008) Soil-column depth-dependent seismic site coefficients and hazard maps for the upper Mississippi Embayment. *Bulletin of the Seismological Society of America* 98: 2004–2021.

Hassani B and Atkinson GM (2016a) Applicability of the site fundamental frequency as a VS30 proxy for central and eastern North America. *Bulletin of the Seismological Society of America* 106: 653–664.

Hassani B and Atkinson GM (2016b) Site-effects model for central and eastern North America based on peak frequency. *Bulletin of the Seismological Society of America* 106: 2197–2213.

Hassani B and Atkinson GM (2018) Site-effects model for central and eastern North America based on peak frequency and average shear wave velocity. *Bulletin of the Seismological Society of America* 108: 338–350.

Hollenback J, Kuehn N, Goulet CA, et al. (2015) *PEER NGA-East median ground-motion models*. PEER report no. 2015/04. Berkeley, CA: Pacific Earthquake Engineering Research Center, University of California.

Hwang HHM and Huo J-R (1994) *Generation of hazard-consistent fragility curves for seismic loss estimation studies*. Technical report NCEER-94-O015. Buffalo, NY: National Center for Earthquake Engineering Research, State University of New York at Buffalo.

Hwang HHM, Lin H and Huo J-R (1997) Site coefficients for design of buildings in eastern United States. *Soil Dynamics and Earthquake Engineering* 16: 29–40.

Kaklamanos J and Bradley B (2018) Challenges in predicting seismic site response with 1D analyses: Conclusions from 114 KiK-net vertical seismometer arrays. *Bulletin of the Seismological Society of America* 108: 2816–2838.

Kwok AO and Stewart JP (2006) Evaluation of the effectiveness of theoretical 1D amplification factors for earthquake ground-motion prediction. *Bulletin of the Seismological Society of America* 96: 1422–1436.

Lin H, Hwang H and Huo J-R (1996) A study on site coefficients for new site categories specified in the NEHRP Provisions. Technical report, Center for Earthquake Research and Information, The University of Memphis, Memphis, TN.

McGuire RK (2004) *Seismic Hazard and Risk Analysis* (EERI Monograph MNO-10). Oakland, CA: Earthquake Engineering Research Institute, p. 187.

Pacific Earthquake Engineering Research Center (PEER) (2015a) *NGA-East: Median ground-motion models for central and eastern North America*. PEER report no. 2015/04. Berkeley, CA: PEER, University of California.

Pacific Earthquake Engineering Research Center (PEER) (2015b) *NGA-East: Adjustments to median ground-motion models for central and eastern North America*. PEER report 2015/08. Berkeley, CA: PEER.

Park D and Hashash YMA (2005a) Evaluation of seismic site factors in the Mississippi Embayment. I. Estimation of dynamic properties. *Soil Dynamics and Earthquake Engineering* 25: 133–144.

Park D and Hashash YMA (2005b) Evaluation of seismic site factors in the Mississippi Embayment. II. Probabilistic seismic hazard analysis with nonlinear site effects. *Soil Dynamics and Earthquake Engineering* 25: 145–156.

Parker GA, Harmon JA, Stewart JP, et al. (2017) Proxy-based VS30 estimation in central and eastern North America. *Bulletin of the Seismological Society of America* 107: 117–131.

Parker GA, Stewart JP, Hashash YMA, et al. (2019) Empirical linear seismic site amplification in central and eastern North America. *Earthquake Spectra* 35: 849–881.

Petersen MD, Moschetti MP, Powers PM, et al. (2015) The 2014 United States national seismic hazard model. *Earthquake Spectra* 31: S1–S30.

Petersen MD, Shumway AM, Powers PM, et al. (2020) 2018 Update of the U.S. National Seismic Hazard Model: Overview of model, changes, and implications. *Earthquake Spectra*.

Romero SM and Rix GJ (2001) *Ground motion amplification of soils in the upper Mississippi Embayment, National Science Foundation Mid America Earthquake Center*. Report no. GIT-CEE/GEO-01-1. Available at: http://hdl.handle.net/2142/8940 (accessed November 2019).

Seyhan E and Stewart JP (2014) Semi-empirical nonlinear site amplification from NGA-West2 data and simulations. *Earthquake Spectra* 30: 1241–1256.

Silva WJ, Abrahamson NA, Toro G, et al. (1997) *Description and validation of the stochastic ground motion model*. Contract No.770573, Brookhaven National Laboratory, Associated Universities, Inc. Upton, NY.

Stafford PJ, Rodriguez-Marek A, Edward B, et al. (2017) Scenario dependence of linear site effect factors for short period response spectral ordinates. *Bulletin of the Seismological Society of America* 107: 2859–2872.

Stewart JP, Afshari K and Goulet CA (2017a) Non-ergodic site response in seismic hazard analysis. *Earthquake Spectra* 33: 1385–1414.

Stewart JP, Parker GA, Harmon JP, et al. (2017b) *Expert panel recommendations for ergodic site amplification in central and eastern North America*. PEER report 2017/04. Berkeley, CA: Pacific Engineering Research Institute.

Stewart JP, Parker GA, Al Atik L, et al. (2019) *Site-to-Site Standard Deviation Model for Central and Eastern North America*. Berkeley, CA: University of California. Available at: https://escholarship.org/uc/item/2sc5g220 (accessed November 2019).

Thompson EM, Baise LG, Tanaka Y, et al. (2012) A taxonomy of site response complexity. *Soil Dynamics and Earthquake Engineering* 41: 32–43.

Xu B, Rathje EM, Hashash YMA, et al. (this issue) κ_0 for soil sites: Observations from Kik-net sites and their use in constraining small-strain damping profiles for site response analysis. *Earthquake Spectra*.